Hindawi
Adsorption Science & Technology
Volume 2022, Article ID 4444164, 15 pages
https://doi.org/10.1155/2022/4444164

Research Article

The Improvement of Natural Thai Bentonite Modified with Cationic Surfactants on Hexavalent Chromium Adsorption from an Aqueous Solution

Nikom Srikacha,[1] Manop Sriuttha,[2] Lamyai Neeratanaphan,[3] Chatree Saiyasombat,[4] and Bundit Tengjaroensakul[1]

[1]*Faculty of Veterinary Medicine, Khon Kaen University, Khon Kaen 40002, Thailand*
[2]*Faculty of Interdisciplinary Studies, Khon Kaen University, Nong Khai Campus, Nong Khai 43000, Thailand*
[3]*Faculty of Science, Khon Kaen University, Khon Kaen 40002, Thailand*
[4]*Synchrotron Light Research Institute, Nakhon Ratchasima 30000, Thailand*

Correspondence should be addressed to Bundit Tengjaroensakul; btengjar@kku.ac.th

Received 14 March 2022; Revised 11 April 2022; Accepted 5 May 2022; Published 21 May 2022

Academic Editor: Senthil Kumar Ponnusamy

This work was performed to evaluate the adsorption properties of modified Thai bentonites (MTBs) on hexavalent chromium (Cr (VI)) by using a popularly capable surfactant (hexadecyltrimethylammonium bromide (HDTMA)) compared to an alternative surfactant (cetylpyridinium chloride (CPC)). The adsorption properties of the surfactant load, adsorbent weight, contact time, initial Cr(VI) concentration, and temperature of the MTBs were evaluated. The results revealed that a higher surfactant load significantly affected the Cr(VI) adsorption, and the equilibrium adsorption was achieved at 60 min. The adsorption capacity improved when the adsorbent weight, contact time, initial concentration, and temperature increased as the highest adsorption capacities of 1CPC and 1HDTMA were 45.55 and 46.03 mg g^{-1}, respectively. The isotherm and kinetic adsorptions were described by the Freundlich model and pseudo-second-order model, respectively, while thermodynamics indicated endothermic adsorption. After adsorption, X-ray absorption near-edge structure and extended X-ray absorption fine structure data showed that Cr ions did not change the valency state between Cr(VI) and Cr(III). Additionally, the adsorption mechanism can be depicted as the ion exchange between the Cr(VI) ion and the surfactant molecule. Structural evaluations by XRD, FTIR, FESEM, EDS, and TEM found that both MTBs (1CPC and 1HDTMA) with the best adsorption performance for Cr(VI) had obvious changes at both the interlayer structure and the external surface. The interlayer spacing was expanded from 14.85 Å to 20.48 Å (1CPC) and 18.79 Å (1HDTMA), and the new functional groups (CH_2 scissoring, C–H symmetric stretching, C–H asymmetric stretching, and N–CH_3 scissoring) and elemental compositions (Br and Cl) were observed in both MTBs. They demonstrated that the complete intercalation of surfactant molecules on bentonite structures supported Cr(VI) adsorption. Overall, the data indicate that MTBs were perfectly adsorbed on Cr(VI), and CPC was demonstrated to be a cheap alternative agent due to its adsorption capacity compared to the popularly capable HDTMA.

1. Introduction

Heavy metal pollution generated by human activities, such as industry, agriculture, commerce, and households, causes concerns and threats to human health and environmental problems in several developing countries, particularly in Thailand [1–3]. Due to incompetent management, municipal solid waste (MSW) from the daily life of society releases various leachate pollutants, especially heavy metals [4, 5]. Furthermore, large quantities of electronic waste (E-waste) contain several heavy metals that are extensively used in various electronic equipment [6]. If they are not safely treated and disposed of, the contamination of heavy metals, including Cr in landfills and E-waste leachate, could be a major

source of water pollution [7, 8]. Previous studies in Thailand discovered abundant Cr contamination and bioaccumulation in the areas around MSW and E-waste [9, 10]. They reported that the concentration of Cr in water, aquatic animals, and edible plants exceeded the Pollution Control Department of Thailand and Food and Agriculture Organization standards [4, 6, 9, 11, 12]. Cr is a natural element where some forms are essential for body functions; however, some forms, especially Cr(VI), are noxious and can induce human health effects, including irritation to the skin and intestinal tract, ulcers, breathing problems, immune suppression, kidney and liver damage, genetic alterations, and death [7, 13, 14]. Several scientists have also reported that Cr(VI) is one of the most common ubiquitous pollutants in aquatic organisms because it induces various adverse effects such as behavioral, physiological, biochemical, histological, genetic, and immunological conditions [15, 16]. From this previous information, a solution to eradicate Cr(VI) contamination in ecosystems is urgently required.

Attention has been focused on developing local and low-cost adsorbents to remove heavy metals from wastewater because the adsorption processes are economical cost, regenerative material, metal selectness, absent generation of toxic sludge, and effectiveness [17, 18]. Among clay-based adsorbents, bentonite is the most generally used in wastewater treatment studies. Bentonite mainly contains montmorillonite which reveals the adsorption efficiency due to its high surface energy and large surface area. However, organic cation surfactants preferably apply several exchangeable cations to bentonite to enhance its adsorption capacity. The modified bentonites demonstrate a better porous structure and a broader interlayer spacing which enhance the heavy metal adsorption capacity [8, 19]. Previous studies reported that modified clays with hexadecyltrimethylammonium bromide (HDTMA) and cetylpyridinium chloride (CPC) increased the adsorption capacity of Cr (VI) by enhancing the ion exchange between the Cr(VI) and the surfactant. Their adsorption capacities on Cr(VI) adsorption were reported to be between 8 and 338 mg g^{-1} [20–24]. Furthermore, clay modified with cetylpyridinium bromide had a higher percentage removal of Cr(VI) from water [25, 26]. In adsorption study results, modified clays showed advantages in solving heavy metal contamination in an aqueous solution; however, the cost should be considered.

From the above information, modified clays with surfactants presented impressive potential on Cr(VI) adsorption, but there have been a few reports on a cheaper agent such as CPC. Consequently, this study is aimed at demonstrating the application of modified Thai bentonites (MTBs) on Cr(VI) adsorption in an aqueous solution by modifying natural Thai bentonite (NTB) with HDTMA and CPC and at comparing their efficiencies and cost considerations. The bentonites were characterized, and mineralogical and structural changes were evaluated. The effects of the surfactant type and dose, adsorbent weight, initial concentration, contact time, and temperature on Cr(VI) adsorption were determined. After adsorption, the change in the Cr valency state and adsorption mechanism were examined. The results of this study can be applied to enhance the treatment of Cr-polluted leachate at municipal and E-waste landfills.

2. Materials and Methods

2.1. Materials. Natural Thai bentonite (NTB) was sieved through mesh No. 40, and its cation exchangeable capacity (CEC) value was 93 cmol kg^{-1}. Hexadecyltrimethylammonium bromide (HDTMA), cetylpyridinium chloride (CPC), and chromium (III) nitrate nonahydrate ($Cr(NO_3)_3{\cdot}9H_2O$, Cr(III)) were purchased from Sigma (USA), and potassium dichromate ($K_2Cr_2O_7$, Cr(VI)) was purchased from Loba Chemie (India). All chemicals were of analytical grade. Deionized (DI) water was used throughout the experiments.

2.2. Bentonite Modification. HDTMA and CPC were utilized to replace the exchangeable cation with NTB as MTBs schematized in Figure 1. The amounts of each surfactant were calculated equally to 0.25CEC, 0.5CEC, and 1CEC of NTB following Chanra et al. [27]. The surfactant was homogeneously dissolved in 100 mL of 10% methanol in a 250 mL conical flask; then, 5 g of NTB was gradually added to each surfactant solution. The suspensions were agitated at 200 rpm for 6 hours at 60°C and subsequently filtered and washed 5 times with deionized (DI) water until free from bromide and chloride ions which can be tested by silver nitrate. MTBs were dried at room temperature for 1 day and subsequently dried at 60°C for 3 hours [28, 29]. The MTBs were set as 0.25CPC, 0.5CPC, 1CPC, 0.25HDTMA, 0.5HDTMA, and 1HDTMA following types and amounts of surfactants.

2.3. Adsorption Experiment and Data Analysis. The adsorption experiments of NTB and MTBs were tested using the batch experiment to evaluate the equilibrium data. The preparation of the adsorbate solution was processed by dissolving $K_2Cr_2O_7$ in DI water adjusted to pH 6, while all adsorption units in this study were shaken in a shaking incubator at 250 rpm. First, the removal of Cr(VI) was conducted using 0.1 g of adsorbents with 25 mL of 50 mg L^{-1} Cr(VI) in a 250 mL conical flask at 25°C for 120 min to measure the adsorption efficiencies of surfactant types and doses. Second, adsorbent weights between 0.1 and 0.3 g were investigated to determine the effect of weight on Cr(VI) adsorption under the same conditions. Third, the effects of initial concentration and contact time were evaluated by mixing 0.1 g of each adsorbent with 100 mL of Cr(VI) at initial concentrations of 12.5, 25, 37.5, 50, and 62.5 mg L^{-1}, while the contact times were 5, 10, 15, 20, 25, 30, 60, and 120 min. Last, the effect of temperature was investigated by performing the effect of temperature at 25, 30, 35, and 40°C with initial concentration and adsorbent weight at 62.5 mg L^{-1} and 0.1 g. At the end of the contact time of each batch adsorption, the solutions were filtered by the Whatman filter paper (No. 1) and nylon syringe filter (13 mm and 0.45 μm). The residual concentration measurement of Cr after adsorption was performed by atomic absorption spectroscopy (PinAAcle 900F, PerkinElmer, USA). The percentage removal (%R) and equilibrium adsorption capacity (q_e) were calculated and expressed as follows:

$$\%R = \frac{(C_0 - C_t)}{C_0} \times 100, \quad (1)$$

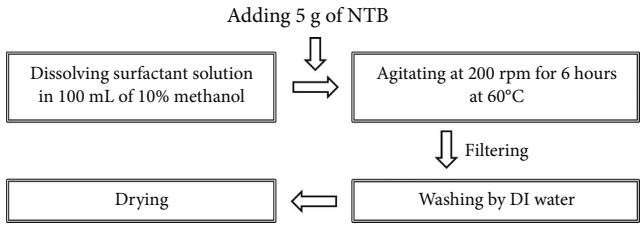

Figure 1: The schematic steps of the MTB modification.

$$q_e = \frac{(C_0 - C_t)}{m} \times v, \quad (2)$$

where %R is the percentage of Cr adsorbed by the adsorbent (%), q_e is the amount of Cr adsorbed by the adsorbent (mg g^{-1}), C_0 is the initial Cr concentration (mg L^{-1}), C_t is the final Cr concentration (mg L^{-1}), m is the adsorbent weight (g), and V is the Cr solution volume (L).

The isotherm study was performed under conditions of an initial Cr(VI) concentration of 12.5–62.5 mg L^{-1}, an adsorbent weight of 0.1 g, a contact time of 60 min, and a temperature of 25°C. The isotherm adsorptions, including Langmuir (Equation (3)), Freundlich (Equation (4)), and Temkin (Equation (5)) models, were analyzed in linear forms by the following equations [30–32]:

$$\frac{1}{q_e} = \frac{1}{K_L q_{max}} \times \frac{1}{C_e} + \frac{1}{q_{max}}, \quad (3)$$

$$\log q_e = \log K_f + \frac{1}{n} \log C_e, \quad (4)$$

$$q_e = \left(\frac{R_T}{b_T}\right) \ln A_T + \left(\frac{R_T}{b_T}\right) \ln C_e, \quad (5)$$

where q_{max} is the amount of Cr(VI) adsorbed (mg g^{-1}) at maximum and K_L (L mg^{-1}) is the constant that presents the interactive relationship of Cr(VI) and the adsorbent. K_L and q_{max} were evaluated from the intercept and slope of $1/C_e$ versus $1/q_e$. K_f is the Freundlich constant, and $1/n$ is the adsorption intensity of the adsorption process. Consequently, the linear line of slope $1/n$ and intercept $\log K_f$ was plotted by $\log q_e$ versus $\log C_e$. A is the equilibrium binding constant that corresponds to the maximum binding energy (L mg^{-1}), and $B = RT/b$ is associated with the adsorption heat. b, R, and T are the Temkin isotherm constant, ideal gas constant (8.314 J mol^{-1} K^{-1}), and absolute temperature in degrees kelvin (K), respectively. A plot of q_e versus $\ln C_e$ determines Temkin constants A and B.

The kinetic study was investigated under conditions of an initial Cr(VI) concentration of 62.5 mg L^{-1}, an adsorbent weight of 0.1 g, a contact time of 0–120 min, and a temperature of 25°C. Kinetic adsorptions were analyzed by pseudo-first-order (Equation (6)), pseudo-second-order (Equation (7)), and intraparticle diffusion (Equation (8)) kinetic models expressed as follows [30, 31, 33]:

$$\ln (q_e - q_t) = \ln q_e - K_1 t, \quad (6)$$

$$\frac{t}{q_e} = \frac{1}{K_2 q_e^2} + \frac{1}{q_e}, \quad (7)$$

$$q_t = K_d t^{1/2} + C, \quad (8)$$

where q_t is the amount of Cr(VI) adsorbed (mg g^{-1}) at time t and the equilibrium rate constant is K_1 (min^{-1}). The slope and intercept of a plot of $\ln (q_e - q_t)$ and t determine the equilibrium adsorption capacity (q_e) and pseudo-first-order rate constant K_1. K_2 (g mg^{-1} min^{-1}) is the equilibrium rate constant. A plot of t/q_t versus t reveals the applicability of the pseudo-second-order model. The values of K_2 and q_e were obtained from the intercept and slope of the plot. K_d (mg g^{-1} min$^{-0.5}$) is the intraparticle diffusion rate constant, and C is the intercept. The plot of q_t versus $t^{1/2}$ demonstrates the values of C and q_t based on the intercept and slope.

The thermodynamic adsorption was calculated from the temperature variations at 298 K, 303 K, 308 K, and 313 K at a constant adsorbent weight (0.1 g), initial concentration (62.5 mg L^{-1}), and contact time (60 min). Thermodynamic parameters were analyzed, including changes in Gibbs free energy (ΔG^0), changes in enthalpy (ΔH^0), and changes in entropy (ΔS^0) for the adsorption process expressed as follows [31]:

$$\Delta G^0 = -RT \ln K_c, \quad (9)$$

$$K_c = \frac{C_a}{C_e}, \quad (10)$$

$$\ln K_c = -\left(\frac{\Delta H^0}{RT}\right) + \left(\frac{\Delta S^0}{R}\right), \quad (11)$$

where T is the temperature (K), R is the ideal gas constant which is 8.314 J mol^{-1} K^{-1}, K_c is the thermodynamic equilibrium constant, C_a (mg L^{-1}) is the concentration of Cr(VI) adsorbed, and C_e (mg L^{-1}) is the equilibrium concentration of Cr(VI) in solution. A linear plot of $\ln K_c$ versus $1/T$ was used to determine the values of ΔH^0 and ΔS^0 based on the slope and intercept.

2.4. X-Ray Absorption Spectroscopy. NTB, 1CPC, and 1HDTMA were subjected to adsorption experiments with Cr(III) and Cr(VI) prepared at 200 mg L^{-1}. Exactly 1 g of each adsorbent was agitated with 25 mL of Cr in a 250 mL conical flask at 25°C for 120 min. At the end, the solutions were filtered by the Whatman filter paper (No. 1) and nylon syringe filter (13 mm and 0.45 μm); then, powder samples were dried at 60°C for 3 hours and sieved through mesh No. 40. Both the solution and powder samples after adsorption were called 1HDTMA+Cr(VI), 1CPC+Cr(VI), 1HDTMA+Cr(III), 1CPC+Cr(III), and NTB+Cr(III). The dried powder samples were loaded in a holder and sealed by Kapton tape, while solution samples were loaded in a plastic zip bag. Cr K-edge spectra of samples and references were obtained at beamline 1.1 W equipped with double crystal monochromator Si(111) at Synchrotron Light Research Institute (SLRI, Thailand). The electron storage energy was 1.2 GeV with a current range of 80–150 mA. The X-ray

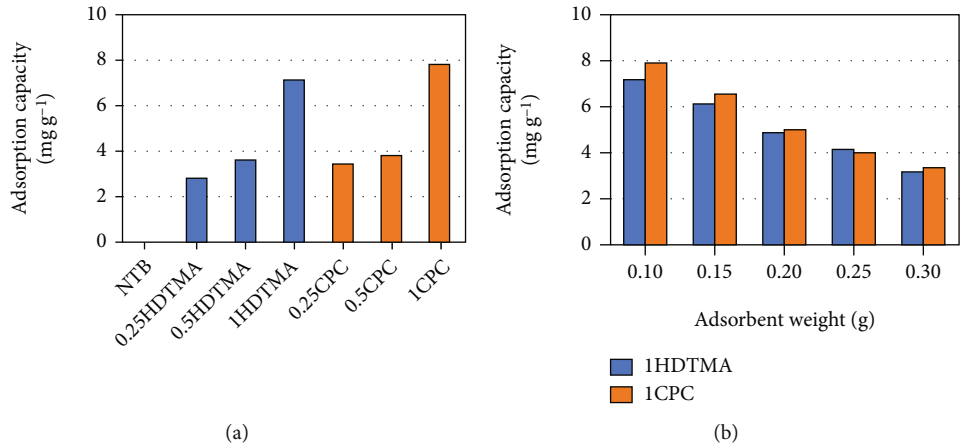

Figure 2: (a) Adsorption capacity of Cr(VI) depending on the surfactant types (CPC and HDTMA) and concentrations (0.25, 0.5, and 1CEC of NTB). (b) Adsorption capacity of Cr(VI) with different MTB weights (0.1–0.3 g).

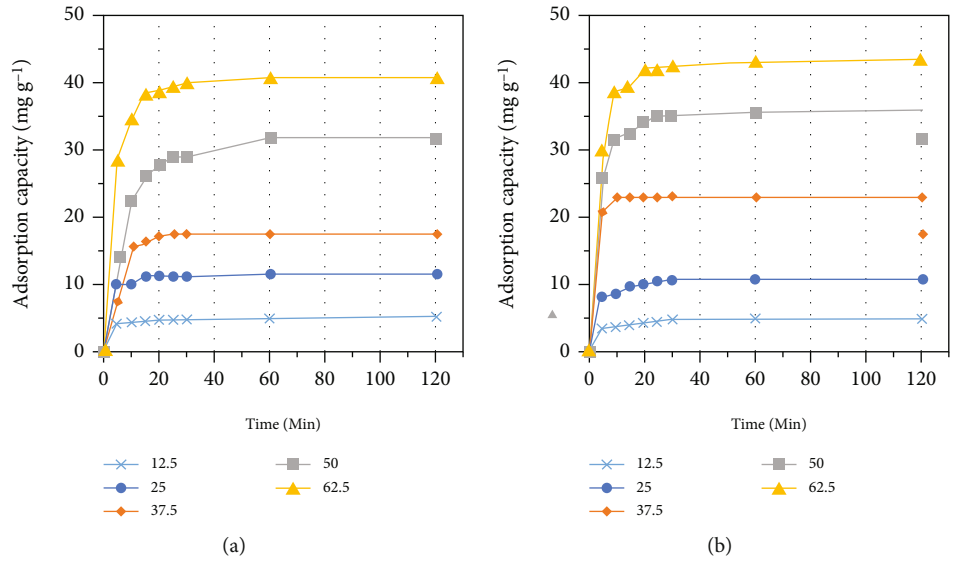

Figure 3: Adsorption capacity of (a) 1CPC and (b) 1HDTMA in a time- and concentration-dependent manner. The adsorption conditions included an initial Cr(VI) concentration of 12.5–62.5 mg L^{-1}, adsorbent weight of 0.1 g, contact time of 0–120 min, and temperature of 25°C.

energy was calibrated by using a metallic Cr foil at 5989 eV. The spectra were recorded in both the fluorescence and transmission modes using a 19-element Ge detector and ionization chamber. X-ray absorption near-edge structure (XANES) and extended X-ray absorption fine structure (EXAFS) spectra were normalized and analyzed using the Athena and Artemis software [34]. To find the coordination number from EXAFS, the amplitude reduction factor ($S0^2$) was fixed at 0.72 according to the fitting result of the Cr foil, while the other values were set as variables.

2.5. Characterization of Adsorbents. The chemical and physical properties were selectively determined on the best performance adsorbent for Cr(VI) adsorption. The functional groups of each adsorbent were measured by Fourier transform infrared (FTIR) spectroscopy (Bruker, TENSOR 27, USA) in transmission mode in the wavenumber range of 500–4,000 cm^{-1}. The mineralogical compositions were determined by X-ray diffraction (XRD) using a D8 Advance X-ray diffractometer (Bruker, USA). The measurement conditions were operated with Cu Kα (λ = 1.5418 Å) radiation in step scan mode at a working voltage and a current of 40 keV and 40 mA, respectively. The angular range was scanned between 2 and 60° (2θ) at a step size of 0.02°/s. The interlayer spacing was calculated using Bragg's law from the 2θ value. The elemental composition and surface morphology of the adsorbents were evaluated by focus ion beam- (FIB-) field emission scanning electron microscopy (FESEM) equipped with an energy-dispersive X-ray spectrometer (EDS) using FEI Helios NanoLab-G3 CX (FEI,

Table 1: Adsorption capacity of Cr(VI) by modified clays with surfactants.

No.	Surfactant	Clay	q_e (mg g^{-1})	Modeling of the adsorption process	Reference
1	HDTMA	Montmorillonite	6.54	Pseudo-second-order model Langmuir model Exothermic adsorption	Hu and Luo [37]
2	HDTMA	Zeolite	337.77	Pseudo-second-order model Dubinin–Radushkevich model Endothermic adsorption	Ghasemi et al. [22]
3	HDTMA	Bentonite	270.30	Pseudo-second-order model Freundlich model	Slimani et al. [54]
4	HDTMA	Bentonite	41.90	Langmuir model	Ramos et al. [55]
5	CPC	Montmorillonite	42.44	Pseudo-second-order model Freundlich model Exothermic adsorption	Zou et al. [23]
6	CPC	Montmorillonite	47.83	Pseudo-second-order model Langmuir model Endothermic adsorption	Liu et al. [24]
7	HDTMA	Bentonite	46.03	Pseudo-second-order model Freundlich model Endothermic adsorption	This study
8	CPC	Bentonite	45.55	Pseudo-second-order model Freundlich model Endothermic adsorption	This study

Table 2: Parameters of the kinetic adsorption analysis.

Kinetic models	Adsorbent	
	1CPC	1HDTMA
qe, exp $(\mathrm{mg\,g^{-1}})$	40.70	43.69
Pseudo-first-order		
qe, cal$(\mathrm{mg\,g^{-1}})$	12.11	13.72
$K_1(\mathrm{min^{-1}})$	0.0814	0.0939
R^2	0.9683	0.9672
Pseudo-second-order		
qe, cal$(\mathrm{mg\,g^{-1}})$	41.17	44.14
h $(\mathrm{mg\,g^{-1}\ min^{-1}})$	33.36	33.22
$K_2(\mathrm{g\,mg^{-1}\ min^{-1}})$	0.02	0.02
R^2	0.9997	0.9997
Intraparticle diffusion		
$K_d(\mathrm{mg\,g^{-1}\,min^{-0.5}})$	2.94	3.16
I	19.32	20.58
R^2	0.5080	0.5086

USA). All samples were coated on the surface by gold sputtering before performing. The microstructure of each sample was determined by transmission electron microscopy (TEM) using TECNAI G^2 20 S-Twin (FEI, USA), operating at 200 keV in imaging modes. The sample powders were prepared by ultrasonically dispersing in deionized water; then, the suspension was dropped on a copper grid.

3. Results and Discussion

3.1. Adsorption Studies on Cr(VI)

3.1.1. Effects of the Surfactant Type and Concentration. NTB was modified with two cation surfactants (HDTMA and CPC) separated into 3 concentrations of each surfactant for Cr(VI) adsorption. Both MTBs had distinctly higher adsorption capacity than NTB (Figure 2(a)). The adsorption data suggest that Cr(VI) adsorption highly depends on the surfactant dose, especially the use of surfactants at 1CEC that is markedly adsorbed on Cr(VI) ions compared to 0.25CEC and 0.5CEC. This may be associated with a number of active and improved adsorption sites when the surfactant concentrations were used [22]. Sarkar et al. [35] revealed that the adsorption capacity of modified bentonite with surfactants on Cr(VI) improved with the concentration of loaded surfactants. The similar adsorption capacities between bentonites modified with CPC and HDTMA occurred due to their similar atomic weight and chemical formula, and they have one atom of the Br or Cl ion in the polar head that can exchange with the Cr(VI) ion. Due to the greater Cr(VI) adsorbed potential than the others, 1HDTMA and 1CPC were selected to investigate different operational factors on the Cr(VI) adsorption. Additionally, the adsorption capability of Cr(VI) onto NTB was discovered to be unsatisfactory. Therefore, further experimental parameters did not proceed in this study. The incompetent performance of NTB on Cr(VI) adsorption can be explained by the electrostatic repulsion between the anionic Cr species and the negatively charged bentonite surface [19]. After modification with cationic surfactants, the bentonite surface and zeta potential shifted from a negative value to a positive value; consequently, the negative Cr(VI) ions interacted with the positive charge of modified bentonite [21, 23, 36].

Table 3: Parameters of the isotherm adsorption analysis.

Isotherm models	Adsorbent	
	1CPC	1HDTMA
Freundlich isotherm		
K_f	0.51	0.21
$1/n$	1.41	1.76
R^2	0.9754	0.9847
Langmuir isotherm		
$q_{max}(\text{mg g}^{-1})$	24.83	15.83
$K_L(\text{L mg}^{-1})$	0.03	0.04
R^2	0.9600	0.9788
Temkin isotherm		
B_T (J mol^{-1})	24.99	30.12
K_T (L mg^{-1})	0.20	0.17
R^2	0.9743	0.9433

Table 4: Parameters of the thermodynamic adsorption analysis.

Adsorbent	T (K)	K_c	ΔG^0 (kJ mol^{-1})	ΔH^0 (kJ mol^{-1})	ΔS^0 (J K^{-1} mol^{-1})
1CPC	298	3.31	-2.97	3.93	23.05
	303	3.29	-3.00		
	308	3.49	-3.20		
	313	3.54	-3.29		
1HDTMA	298	3.38	-3.02	1.19	14.02
	303	3.34	-3.04		
	308	3.38	-3.12		
	313	3.45	-3.22		

Table 5: Cr concentration in the sample after adsorption.

Cr valency state	Adsorbent	Concentration of Cr in powder (mg g^{-1})	Concentration of Cr in solution (mg L^{-1})
Cr(VI)	1CPC	37.22	130.77
	1HDTMA	43.94	113.93
Cr(III)	NTB	71.69	69.87
	1CPC	60.12	93.01
	1HDTMA	53.75	105.75

Furthermore, Hu and Luo [37] proposed chemical equations that imply that the adsorptions of Cr(VI) on modified bentonite corresponded to the surface complexation reaction with HDTMA+ or CPC+ incorporated with Al–O$^-$ and Si–O$^-$ on the bentonite surface. HDTMA+ or CPC+ combined with Cr(VI) is a "bridge" called "bridge efforts" [37].

3.1.2. Effect of Adsorbent Weight. To demonstrate an appropriate adsorbent weight of MTBs on Cr(VI) adsorption, the effect of adsorbent weight was performed in the range of 0.1–0.3 g. Interestingly, both MTBs had equal adsorption patterns, while the highest adsorption capacity was 1CPC (7.87 mg g^{-1}) followed by 1HDTMA (7.14 mg g^{-1}) at 0.1 g (Figure 2(b)). According to the result of 0.1 g with the highest adsorption capacity, 0.1 g of each adsorbent was selected to determine the effect of the contact time, initial Cr(VI) concentration, and temperature. Previous studies reported the continuous reduction of adsorption capacity following the increase of adsorbent weight [22, 31, 38]. The reduction of adsorption capacity was discovered when the adsorbent weight was increased. This decrease responded to the higher adsorbent weight that presented more unsaturated adsorption sites during the adsorption process [22, 31].

Table 6: EXAFS and Fourier transform spectral fitting.

Sample	Shell	N	R (Å)	σ^2
Cr(VI) standard	Cr–O	3.75	1.63	0.004
Cr(III) standard	Cr–O	5.75	1.96	0.003
NTB+Cr(III)	Cr–O	5.60	1.97	0.001
1CPC+Cr(III)	Cr–O	5.41	1.96	0.002
1HDTMA+Cr(III)	Cr–O	5.67	1.97	0.002
1CPC+Cr(VI)	Cr–O	3.65	1.64	0.002
1HDTMA+Cr(VI)	Cr–O	3.69	1.63	0.001

N = number of neighbor atoms; R = interatomic distance; σ^2 = Debye–Waller factor.

3.1.3. Effect of Contact Time. Figure 3 shows that the adsorption rate performed well in a short period of contact time within 30 min, the adsorption rate results slightly increased, and equilibrium was attained at 60 min for all samples. This result was similar to a previous study that reported that montmorillonite modified with CPC reached equilibrium within around 60 min after interaction with Cr(VI) [24]. Both MTBs presented similar adsorption patterns and efficacies. Rapid Cr(VI) adsorption can imply the combination of physical and chemical adsorptions on the adsorption progress, especially for physical adsorption during rapid adsorption progress [19, 37] and the accessibility of large amounts of vacant active sites [39]. Additionally, the inability of adsorbents to remove Cr(VI) at the later stages can indicate the limitation of active sites and slow diffusion of Cr(VI) ions to the interior of the bentonite surface which became full as time progressed [8, 31]. Pasgar et al. [40] informed that the repulsive force between metal ions inside adsorbent surfaces and remaining ions limits metal ion adsorption; consequently, the adsorption rate decreased over time until it reached equilibrium. Liu et al. [24] and Hu and Luo [37] reported that montmorillonite modified with CPC and HDTMA had a quick adsorption rate reaching equilibrium within 60 min.

3.1.4. Effect of Initial Cr(VI) Concentration. The increase in initial Cr(VI) concentration from 12.5 to 62.5 mg L^{-1} extended the adsorption efficacy, as expected. Obviously, the Cr(VI) adsorption at 62.5 mg L^{-1} presented the highest adsorption capacity for both MTBs (Figure 3). At a low initial concentration, Cr(VI) ions did not cover all active sites;

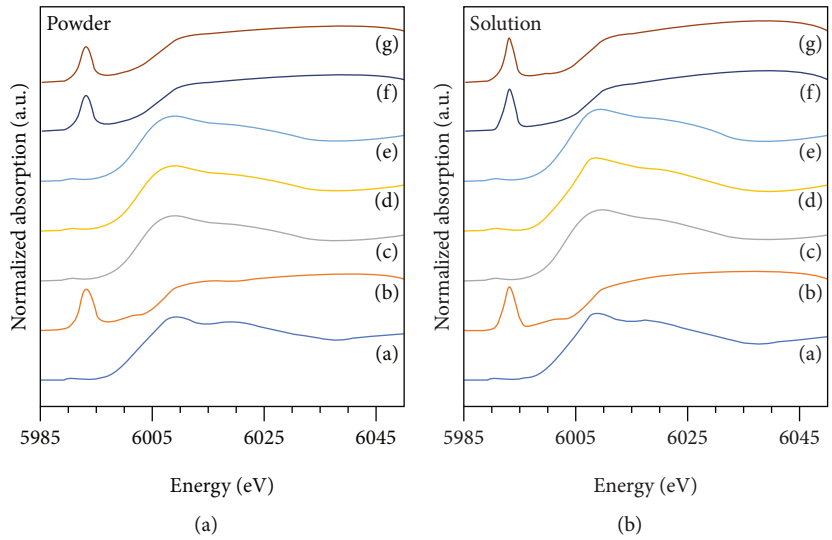

Figure 4: Preedge feature of normalized Cr K-edge XANES spectra of references and samples included the (a) Cr(III) reference, (b) Cr(VI) reference, (c) NTB+Cr(III), (d) 1HDTMA+Cr(III), (e) 1CPC+Cr(III), (f) 1HDTMA+Cr(VI), and (g) 1CPC+Cr(VI).

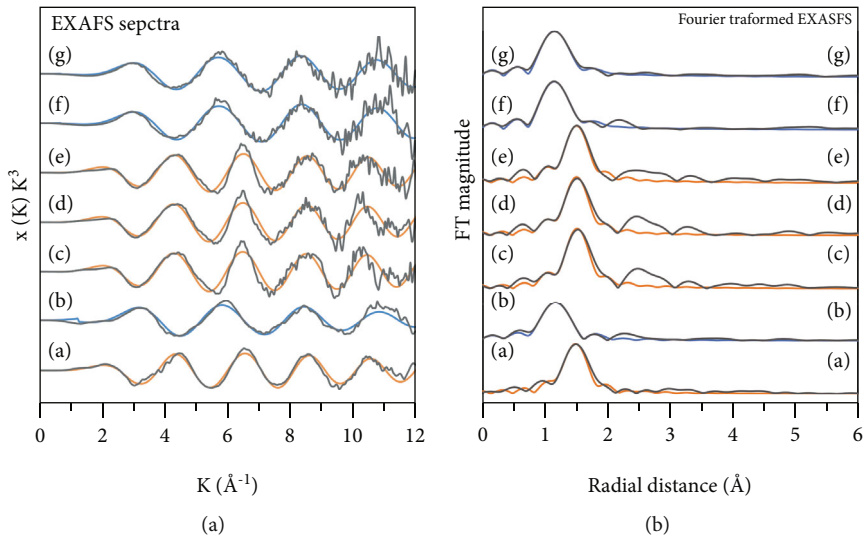

Figure 5: EXAFS spectra and Fourier transform EXAFS of powder references and powder samples included the (a) Cr(III) reference, (b) Cr (VI) reference, (c) NTB+Cr(III), (d) 1HDTMA+Cr(III), (e) 1CPC+Cr(III), (f) 1HDTMA+Cr(VI), and (g) 1CPC+Cr(VI). The black lines are raw data, and the color lines are fitted data.

consequently, the interaction between Cr(VI) and the active site of the adsorbent was not accomplished for maximum adsorption, and when Cr(VI) concentration increased, more Cr(VI) ions extremely covered these sites [41]. From these results, Cr(VI) ions were maximally adsorbed on active sites which presented higher adsorption per unit mass of adsorbent or adsorption capacity. The active sites could remain after Cr(VI) adsorption at lower concentrations, but these sites could be saturated to a stable adsorption capacity at higher concentrations [31, 42].

3.1.5. Effect of Temperatures. The results of the temperature parameters on Cr(VI) adsorption reveal that the adsorption of both MTBs gradually increased with increasing temperature. The adsorption capacities at 25, 30, 35, and 40°C were 40.15, 40.07, 43.33, and 45.55 mg g^{-1} for 1CPC and 42.52, 42.67, 43.91, and 46.03 mg g^{-1} for 1HDTMA, respectively. At higher temperatures, the Cr(VI) ions theoretically acquired higher energy to overcome the energy barrier between the Cr(VI) and the adsorbent which simultaneously created more additional adsorption sites on the adsorbent surface due to the dissociation of some surface components on modified bentonite [31]. Ghasemi et al. [22] and Liu et al. [24] discovered the endothermic adsorption of clay modified with CPC and HDTMA on Cr(VI) adsorption (Table 1). In contrast, Hu and Luo [37] reported that the adsorption of Cr ions decreased at higher temperatures because the surfactant desorbed from the bentonite surface

Table 7: The comparison of chemical and physical characteristics.

No.	Clay	Agent	CEC	*D*-spacing (Å)	New FTIR bands (cm^{-1})	Reference
1	Bentonite	CPC	0	14.99	1465, 1490, 2852, 2926	Banik et al. [68]
			1	16.97		
2	Montmorillonite	CPC	0	14.70	1468, 2847, 2916	Zou et al. [23]
			1	19.30		
3	Montmorillonite	CPC	0	15.30	1468, 2847, 2916	Liu et al. [24]
			1	23.60		
4	Montmorillonite	HDTMA	0	12.67	2850, 2920	Zawrah et al. [69]
			1	19.80		
5	Montmorillonite	HDTMA	0	12.60	—	Abdel-Wahhab et al. [70]
			1	19.80		
6	Montmorillonite	HDTMA	0	15.17	2850, 2918	Hu and Luo [37]
			1	22.50		
7	Bentonite	CPC	0	14.85	1465, 1486, 2851, 2924	This study
			1	20.48		
8	Bentonite	HDTMA	0	14.85	1465, 1486, 2851, 2924	This study
			1	18.79		

0CEC = natural clay without modification; *D*-spacing = the value from XRD. FTIR bands at 1465–1468, 1486–1490, 2847–2852, and 2916–2926 cm^{-1} corresponded to CH_2 scissoring, N–CH_3 scissoring, C–H symmetric stretching, and C–H asymmetric stretching, respectively.

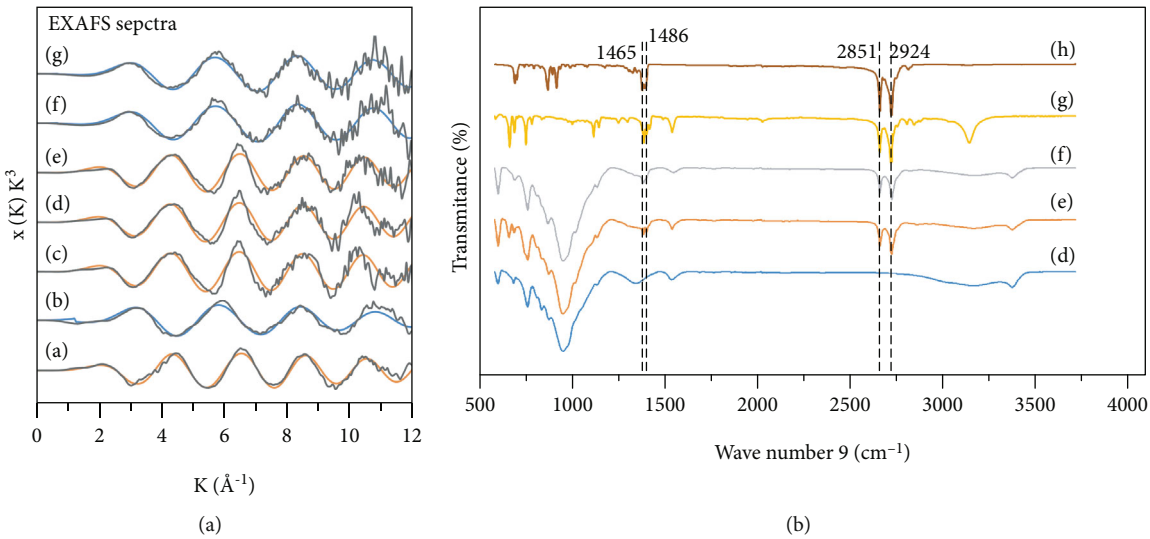

Figure 6: (a)–(c) X-ray diffractograms of NTB, 1CPC, and 1HDTMA, respectively. (d)–(h) FTIR spectra of NTB, 1CPC, 1HDTMA, CPC, and HDTMA, respectively.

when the solution temperature increased. They suggested that the Cr(VI) adsorption by surfactant-modified bentonite should be performed at lower temperatures.

3.1.6. Kinetic Adsorption. The kinetic calculation results of both MTBs among 3 models, including pseudo-first-order, pseudo-second-order, and intraparticle diffusion models, show consistency between experimental adsorption capacity ($q_{e,exp}$) and calculated adsorption capacity ($q_{e,cal}$) of the pseudo-second-order model (Table 2). Additionally, the R^2 values were all greater than the other 2 models which indicates that the adsorption process can be reported as a pseudo-second-order model. This result suggests that the adsorption between both MTBs and Cr(VI) ions was chemical adsorption involving ion sharing or exchange between the Cr(VI) and the adsorbent [8, 30, 43]. The equal rate constant (K_2) reveals that the adsorption of 1CPC was as fast as 1HDTMA, and the equal initial adsorption rate (h) results in similar active sites that could readily adsorb Cr(VI) ions [35]. The chemical adsorption between the modified bentonite and the Cr(VI) ion is associated with Hu and Luo [37] and Zou et al. [23] presented in Table 1.

3.1.7. Isotherm Adsorption. To investigate the best fitting isotherm, Langmuir, Freundlich, and Temkin models were calculated at equilibrium adsorption (Table 3). The results

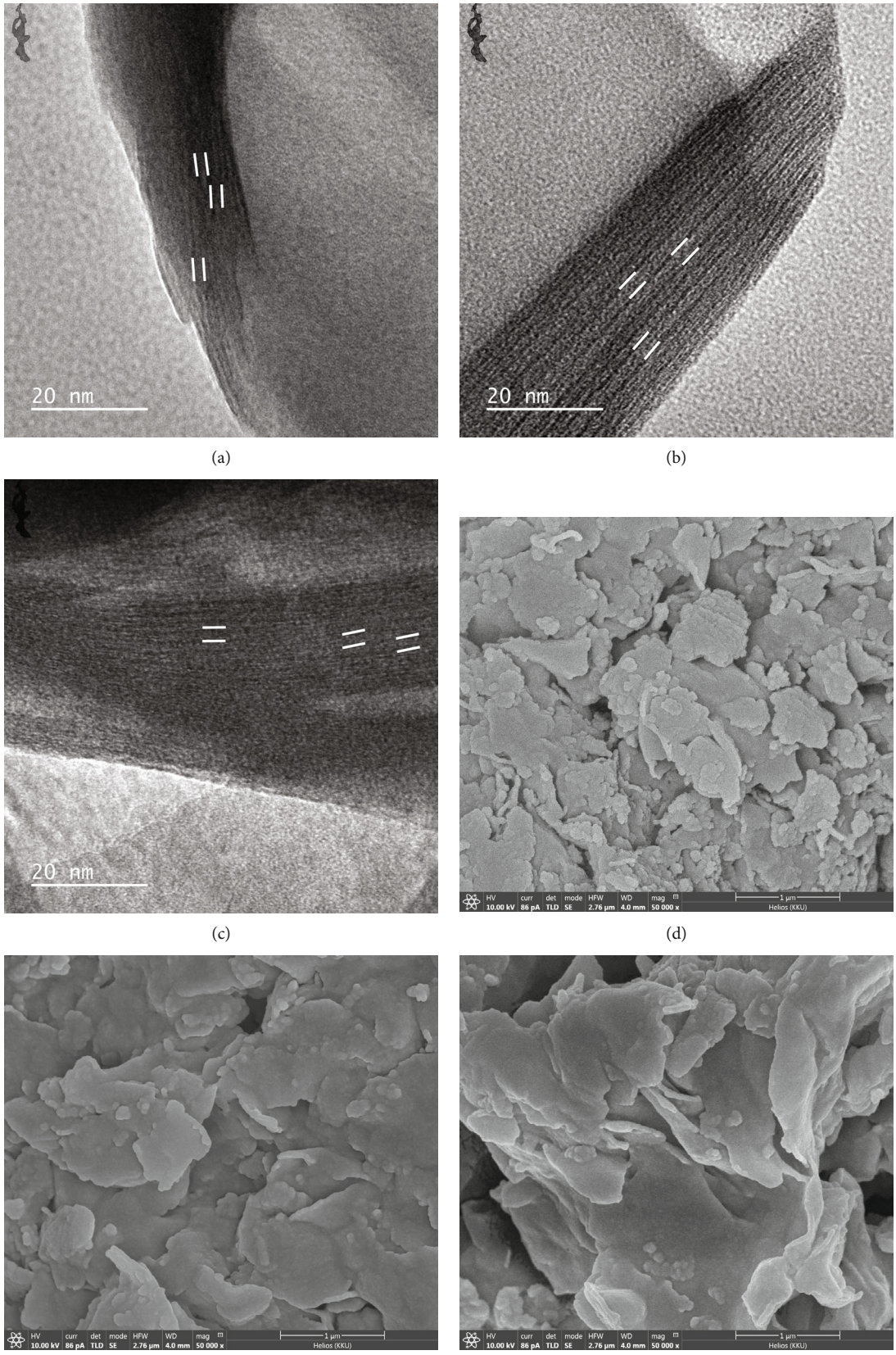

(a) (b) (c) (d) (e) (f)

Figure 7: TEM images of (a) NTB, (b) 1CPC, and (c) 1HDTMA (scale bar = 20 nm). (d)–(f) FESEM microphotographs of NTB, 1CPC, and 1HDTMA, respectively (50,000x magnification).

Table 8: Elemental composition (%) of NTB, 1CPC, 1HDTMA, and MTBs after Cr(VI) adsorption.

Elemental composition (K)	Adsorbent				
	NTB	1CPC	1HDTMA	1CPC +Cr(VI)	1HDTMA +Cr(VI)
O	51.2	23.9	30.7	33.6	34.3
Ca	25.2	0.9	11.3	1.0	0.1
C	13.1	40.2	35.2	31.9	36.9
Si	7.2	23.6	15.7	24.4	21.2
Al	2.0	6.8	3.0	5.6	4.2
Mg	1.0	1.5	0.6	0.9	0.7
Fe	0.4	1.4	1.9	1.0	0.6
Cl	0.0	1.7	0.0	0.0	0.0
Br	0.0	0.0	1.6	0.0	1.3
Cr	0.0	0.0	0.0	1.0	0.7

show that the R^2 values of both adsorbents were similar among 3 isotherms; however, the isotherm was fitted better with the Freundlich model indicating that the Cr(VI) adsorption process was multilayer adsorption by the heterogeneous adsorbent [8, 43]. Additionally, $1/n$ higher than 1 indicated an unfavorable adsorption reaction [43, 44]. Zou et al. [23] also discovered the similarity of R^2 among 3 isotherms ranging between 0.97 and 0.98; however, the isotherm fitted better with the Freundlich model (Table 1).

3.1.8. Thermodynamics. The thermodynamic parameters are reported in Table 4. The thermodynamic adsorption was examined at 298 K, 303 K, 308 K, and 313 K. The K_c values slightly increased when the temperature increased for both MTBs. The Cr(VI) adsorptions on both MTBs were totally an endothermic process according to all positive values of ΔH^0 indicating that the adsorption increased when temperatures increased, and they showed the possible strong bonding between the adsorbent and the Cr(VI). The negative values of ΔG^0 at all temperatures displayed the feasibility and spontaneity of the adsorption process. Furthermore, the enhanced disorder and randomness at the solid-solution interface of Cr(VI) with the adsorbent were confirmed by the positive values of ΔS^0 [31, 45–48]. The thermodynamic and spontaneous adsorption processes between MTBs and Cr(VI) were similar to previous studies that investigated the adsorption behavior between surfactant-modified bentonite and Cr(VI) [23, 24, 26] (Table 1).

Based on the above results, 1CPC and 1HDTMA showed the highest adsorption of Cr(VI) under the optimal conditions such as an initial Cr(VI) concentration of 62.5 mg L^{-1}, an adsorbent weight of 0.1 g, a temperature of 40°C, and a contact time of 60 min. 1CPC and 1HDTMA can distinctly adsorb the Cr(VI) ion under the optimal conditions presenting adsorption capacity at 45.55 and 46.03 mg g^{-1} or percentage removal at 71.72 and 85.21%, respectively, while NTB cannot adsorb Cr(VI). These results were compared to prior reports in Table 1. After the adsorption study with the synthetic sample, the investigation with real sample conditions (real wastewater) should be performed. Pasgar et al. [40] and Honarmandrad et al. [49] discovered the reduction of percentage removal in real sample conditions due to the impurities in this sample, including the turbidity, total suspended solid, and sulfate ion. Therefore, the percentage removal in the real sample is less than that in the synthetic sample. These results are an advantage for future applications in wastewater treatment. Previous studies suggested that the adsorbents after adsorbing Cr(VI) can be reused by desorbing adsorbate with several methods [50–53]. For example, the adsorbent immersed in the 0.1 M NaOH solution can desorb Cr(VI) at 61–82% [50, 51]. Additionally, the desorption or digestion of adsorbent can separate the adsorbate to eliminate by standard methods.

3.2. Determination of the Cr(VI) Adsorption Mechanism. The Cr(III) and Cr(VI) concentrations in powder and solution samples after adsorption are presented in Table 5. The XANES spectra from the Cr K-edge of the samples were compared with the corresponding spectra of two Cr references to investigate the valency state (Figure 4). The Cr (VI) reference shows a distinct preedge peak feature at 5993 eV which indicates Cr(VI) characteristics, while this peak is absent in the Cr(III) reference which represents pure Cr(III) [56, 57]. The XANES spectra of Cr(III) of both the solution and powder samples adsorbed by NTB, 1HDTMA, and 1CPC revealed the absence of a preedge peak at 5993 eV, and the strong adsorption peak revealed a maximum at 6009 eV. According to this result, no significant Cr(VI) was reported in these samples. In contrast, the XANES spectra of Cr(VI) of both the solution and powder samples after adsorption by 1HDTMA and 1CPC showed a strong peak similar to the Cr(VI) reference. These results confirm that neither Cr(III) nor Cr(VI) significantly changed the valency state after adsorption with NTB and MTBs. A previous study reported that the forms of Cr(III) at pH 4.2–12 were Cr_2O_3 and minor $Cr(OH)_3$ [58]. These cation forms in the bulk solution were exchangeable with polycations of the bentonite surface, including Ca^{2+}, Mg^{2+}, Na^+, and K^+ cations [59]. In terms of Cr(VI) in the pH range of 2–7, $HCrO_4^-$ and $Cr_2O_7^{2-}$ ions were the negatively dominant forms. The most presumed reactions that report the adsorption of Cr(VI) anions on the modified clays were ion exchange or electrostatic interaction with Cr(VI) forms such as clay-$(HDTMA)_2HCrO_4$ and clay-$(HDTMA)Cr_2O_7$ [20, 60]. The transformation of Cr(VI) to Cr(III) after adsorption can be explained by the electron donor of the adsorbent providing electrons to the Cr ion [23, 61]. This reduction reaction revealed the decrease in peak height of the preedge that was absent in this study [62]. Wu et al. [63] reported that modified montmorillonite-iron nanoparticles with HDTMA reduced the Cr valency state to a lower poisonous form after adsorption according to the interaction between the Cr(VI) ion and the Fe^0. Zou et al. [23] discovered that the adsorption of Cr(VI) by montmorillonite modified with CPC/Keggin-Al_{30} reduced the valency state to Cr(III) by a large number of hydroxyl (contributed from Al_{30}). Overall, the adsorption in this study was the exchange of polycations on the bentonite surface or surfactant ions between Cr(VI)

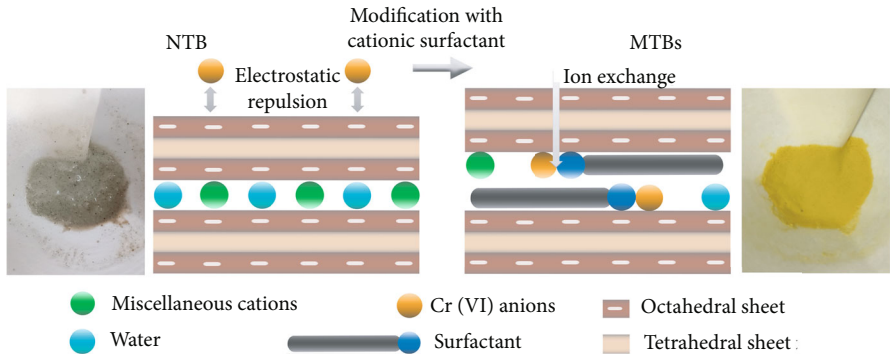

Figure 8: Adsorption mechanisms of Cr(VI) onto modified Thai bentonites.

and Cr(III); consequently, the Cr valency state did not significantly change after adsorption.

To determine the local atomic structure of Cr inside the adsorbent structure, EXAFS analysis was performed. The Cr K-edge EXAFS and Fourier transform spectra are presented in Figure 5, and the fitted values are listed in Table 6. The reference of Cr(III) presents a coordination shell of 5.75 oxygen atoms with a single Cr–O interatomic distance at 1.96 Å which presents an octahedral configuration, while the Cr (VI) reference is tetrahedral coordination with 3.75 oxygen atoms at 1.63 Å. These results are similar to previous reports [62, 64, 65]. The fitted data of all samples after adsorbing Cr showed a strong peak of Cr–O coordination in the first shell, while the second-shell peaks were noted but not included in the fitting due to their unclear characteristics. The adsorbents after adsorbing Cr(III) were satisfactorily fitted to Cr–O at a distance of 1.96–1.97 Å with oxygen around 5.41–5.67 atoms, but the MTBs adsorbing Cr(VI) were satisfactorily fitted with oxygen at 1.63–1.64 Å around 3.65–3.69 atoms. These results also suggest that the valency state of Cr did not change after it interacted with the adsorbents because the coordination environment of Cr in these samples was similar to references as well as their characteristics. Additionally, as the adsorption mechanism likely depicted the interaction between the Cr(VI) ion and the surfactant molecule, the absence of the dominant second shell in fitted data indicated that ion exchange or outer-sphere complexation is mainly responsible for the adsorption of Cr(VI) by MTBs [57]. This result was associated with previous studies that reported that the adsorption mechanism between Cr (VI) and modified bentonite was the ion exchange between Cr(VI) and Br or Cl ions inside the interlayer [23, 25, 26].

3.3. Chemical and Physical Characteristics of Adsorbents. The chemical and physical properties were selectively determined on the best performance adsorbent for Cr(VI) adsorption, and these results were compared to previous studies in Table 7. Due to the high sensitivity to changes in crystallinity, XRD was performed to compare the difference before and after modification (Figures 6(a)–6(c)). The X-ray diffractogram of the NTB showed the strong peak ($d(001)$) of montmorillonite which is the main mineral in bentonite at the 2 theta of 5.95° (14.85 Å). After modification, the surfactant clearly expanded the interlayer spacing when the 2 theta values decreased. The insertion of cation surfactants in the interlayer of bentonite was suggested by an increase in basal spacing to 20.48 Å at 4.32° for 1CPC and 18.79 Å at 4.70° for 1HDTMA (Figures 6(b) and 6(c)). The differently cationic surfactant intercalating in the interlayer of bentonite showed a difference in basal spacing which varied with the nature and concentration of the surfactant. The intercalation in the interlayer of the bentonite lattice was affirmed by an increase in basal spacing and a decrease in the 2 theta value of the bentonite modified with cation surfactants [66]. In an aqueous solution, alkylammonium ions or quaternary ammonium cations can be maintained by both the interlayer and outer surfaces of bentonite via an ion exchange process. These ions were not easily displaced by smaller cations such as H^+ and Na^+ [67]. The expansion of basal spacing of clay after intercalating with the surfactant at 1CEC was similar to previous studies summarized in Table 7.

Different functional groups between NTB and MTBs were confirmed by the FTIR spectra in Figures 6(d)–6(h). The main functional groups of bentonites such as Si–O bond stretching vibrations presented at approximately 619, 792, and 999 cm^{-1}, while peaks at 711, 917, and 3621 cm^{-1} corresponded to Si–O–Si, Al–Al–OH, and O–H asymmetric stretching, respectively [71–73]. Additionally, the band at approximately 1633 cm^{-1} was ascribed to water molecule or H–O–H bending [74]. After modification with both cation surfactants, new bands appeared, as represented by dashed lines at 1465, 2851, and 2924 cm^{-1} presenting CH_2 scissoring, C–H symmetric stretching, and C–H asymmetric stretching, respectively, while the small band at 1486 cm^{-1} of N–CH_3 scissoring was only found in CPC modification [73, 74]. The occurrence of new bands was associated with pure surfactant spectra indicating the intercalation of the surfactant in both MTBs (Figures 6(g) and 6(h)). Zawrah et al. [69] and Hu and Luo [37] discovered that modified clay with HDTMA at 1CEC presented 2 new functional groups, while Banik et al. [68], Zou et al. [23], and Liu et al. [24] found 3-4 functional groups after clay intercalating with CPC at 1CEC (Table 7).

Figures 7(a)–7(c) display TEM images in which the surfactant clearly enlarged the basal spacing of the MTBs compared to the NTB. This result was associated with XRD analysis that the surfactant was very effective in expanding

the clay layer [75]. The average interlayer spacing measurements of 1CPC and 1HDTMA were 20.80 and 18.84 Å, respectively, while NTB was 14.86 Å. The positively charged head group of the surfactant cation powerfully and electrostatically interacted with the negatively charged clay surface. Then, the head group of the surfactant cation could hold close to the clay surface. Since the surfactants were equally loaded to 1CEC, the interlayer spacing of MTBs was 19–20 Å; thus, the intercalation of the surfactant between the silicate layers was complete as a bilayer [67, 76]. The FESEM images of NTB and MTBs presented the surface morphology at a magnification of 50,000 (Figures 7(d)–7(f)). The MTB composite featured a larger particle size than NTB, while the NTB presented a small flake with a rough surface. After modification, MTBs showed significant morphological changes, including larger particles, smoother surfaces, and swollen and fluffier morphologies. These results indicate that the interlayer space and surface feature of the MTBs strongly depend on the packing density of the surfactants in the interspace of bentonite [77]. The hydrophobic tails of the surfactant laterally interacted on the bentonite surfaces which formed large particles with relatively smooth surfaces [67]. Elemental composition was conducted to prove the presence of different elements between NTB and MTBs by energy-dispersive X-ray spectroscopy (EDS) (Table 8). The EDS of all samples presented the primary chemical compositions of bentonite, including O, Ca, C, Si, Al, Mg, and Fe. The higher C in MTBs indicated the long alkyl chains of the surfactant that was adsorbed by bentonite as well as Br and Cl. In contrast, the lower Ca may be the displacement of surfactant cations between bentonite layers [72]. After Cr(VI) adsorption, Cr composition appeared in both MTBs, while Br and Cl decreased. Therefore, the ion exchange mechanism between the Cr(VI) ion and the Br or Cl ion in batch adsorption can be confirmed [19, 23, 24].

4. Conclusions

This study can conclude that CPC reveals similar performance to HDTMA as modified agents; consequently, CPC can be an alternative surfactant because it is cheaper than HDTMA. With apparent adsorption efficacy, the Cr(VI) adsorption rapidly reached equilibrium at 60 min, and the adsorption capacity was higher when the surfactant load, adsorbent weight, contact time, initial concentration, and temperature increased. The kinetic adsorption was distinctly narrated by the pseudo-second-order model, while the isotherm adsorption was fitted with the Freundlich model. Endothermic adsorption was observed when the temperature increased. The valency states of both Cr(III) and Cr (VI) did not change after interacting with MTBs, and the adsorption mechanism between Cr(VI) and MTBs was the ion exchange between Cr(VI) and the surfactant cation inside the interlayer as confirmed by XANES and EXAFS data. The chemical and physical characteristics found that surfactants play an important role in the interlayer and surface changes of MTBs that were successfully employed to enhance Cr(VI) adsorption (Figure 8).

Data Availability

Data of this paper are available on request to the corresponding author.

Conflicts of Interest

The authors declared no potential conflicts of interest with respect to the research, authorship, and/or publication of this article.

Acknowledgments

This work was supported by a research fund for supporting lecturers to admit a high-potential student to study and research on his expert program year 2018, Graduate School, Khon Kaen University (612H225), a research program on high-performance researchers, Faculty of Veterinary Medicine, Khon Kaen University, and a research program on toxic substances, microorganisms, and feed additives for food safety, Khon Kaen University, Thailand.

References

[1] Y. Liu, X. Ke, X. Wu et al., "Simultaneous removal of trivalent chromium and hexavalent chromium from soil using a modified bipolar membrane electrodialysis system," *Environmental Science & Technology*, vol. 54, no. 20, pp. 13304–13313, 2020.

[2] K. Zuo, X. Huang, X. Liu et al., "A hybrid metal-organic framework-reduced graphene oxide nanomaterial for selective removal of chromate from water in an electrochemical process," *Environmental Science & Technology*, vol. 54, no. 20, pp. 13322–13332, 2020.

[3] Z. Honarmandrad, N. Javid, and M. Malakootian, "Efficiency of ozonation process with calcium peroxide in removing heavy metals (Pb, Cu, Zn, Ni, Cd) from aqueous solutions," *Applied Sciences*, vol. 2, no. 4, 2020.

[4] M. Sriuttha, B. Tengjaroenkul, S. Intamat, U. Phoonaploy, P. Thanomsangad, and L. Neeratanaphan, "Cadmium, chromium, and lead accumulation in aquatic plants and animals near a municipal landfill," *Human and Ecological Risk Assessment*, vol. 23, no. 2, pp. 350–363, 2016.

[5] N. Yukalang, B. D. Clarke, and K. E. Ross, "Solid waste management in Thailand: an overview and case study (Tha Khon Yang sub-district)," *Reviews on Environmental Health*, vol. 32, no. 3, pp. 223–234, 2017.

[6] P. Thanomsangad, B. Tengjaroenkul, M. Sriuttha, and L. Neeratanaphan, "Heavy metal accumulation in frogs surrounding an e-waste dump site and human health risk assessment," *Human and Ecological Risk Assessment*, vol. 26, no. 5, pp. 1313–1328, 2020.

[7] H. S. Kim, Y. J. Kim, and Y. R. Seo, "An overview of carcinogenic heavy metal: molecular toxicity mechanism and prevention," *Journal of Cancer Prevention*, vol. 20, no. 4, pp. 232–240, 2015.

[8] G. Wang, Y. Hua, X. Su, S. Komarneni, S. Ma, and Y. Wang, "Cr(VI) adsorption by montmorillonite nanocomposites," *Applied Clay Science*, vol. 124-125, pp. 111–118, 2016.

[9] U. Phoonaploy, S. Intamat, B. Tengjaroenkul, M. Sriuttha, A. Tanamtong, and L. Neeratanaphan, "Evaluation of Abnormal Chromosomes in Rice Field Frogs (Fejervarya

limnocharis) from Reservoirs Affected by Leachate with Cadmium, Chromium and Lead Contamination," *EnvironmentAsia*, vol. 9, no. 2, 2016.

[10] L. Neeratanaphan, S. Khamma, R. Benchawattananon, P. Ruchuwararak, S. Appamaraka, and S. Intamat, "Heavy metal accumulation in rice (Oryza sativa) near electronic waste dumps and related human health risk assessment," *Human and Ecological Risk Assessment*, vol. 23, no. 5, pp. 1086–1098, 2017.

[11] P. Ruchuwararak, S. Intamat, B. Tengjaroenkul, and L. Neeratanaphan, "Bioaccumulation of heavy metals in local edible plants near a municipal landfill and the related human health risk assessment," *Human and Ecological Risk Assessment: An International Journal*, vol. 25, no. 7, pp. 1760–1772, 2018.

[12] U. Phoonaploy, B. Tengjaroenkul, and L. Neeratanaphan, "Effect of heavy metals from an electronic waste open dumping area on the cytotoxicity of climbing perch (Anabas testudineus)," *International Journal of Environmental Studies*, vol. 77, pp. 1–15, 2020.

[13] K. Kocadal, F. B. Alkas, D. Battal, and S. Saygi, "Cellular pathologies and genotoxic effects arising secondary to heavy metal exposure: a review," *Human and Experimental Toxicology*, vol. 39, no. 1, pp. 3–13, 2020.

[14] M. Ahmadian, M. Malakootian, N. Yousefi et al., "Nickel (II) removal from industrial plating effluent by Fenton process," *Environmental Engineering and Management Journal*, vol. 14, no. 4, pp. 837–842, 2015.

[15] Y. Awasthi, A. Ratn, R. Prasad, M. Kumar, and S. P. Trivedi, "An _in vivo_ analysis of Cr^{6+} induced biochemical, genotoxicological and transcriptional profiling of genes related to oxidative stress, DNA damage and apoptosis in liver of fish, _Channa punctatus_ (Bloch, 1793)," *Aquatic Toxicology*, vol. 200, pp. 158–167, 2018.

[16] A. Bakshi and A. K. Panigrahi, "A comprehensive review on chromium induced alterations in fresh water fishes," *Toxicology Reports*, vol. 5, pp. 440–447, 2018.

[17] D. M. Singh and D. S. Verghese, "Conventional and innovative techniques for removal of heavy metals from electroplating industry waste water," *International Journal of Engineering Sciences & Research Technology*, vol. 5, no. 10, pp. 150–159, 2016.

[18] A. Tripathi and M. Ranjan, "Heavy metal removal from wastewater using low cost adsorbents," *Journal of Bioremediation & Biodegradation*, vol. 6, no. 6, pp. 1–5, 2015.

[19] S. I. Rathnayake, W. N. Martens, Y. Xi, R. L. Frost, and G. A. Ayoko, "Remediation of Cr (VI) by inorganic-organic clay," *Journal of Colloid and Interface Science*, vol. 490, pp. 163–173, 2017.

[20] A. Gładysz-Płaska, M. Majdan, S. Pikus, and D. Sternik, "Simultaneous adsorption of chromium(VI) and phenol on natural red clay modified by HDTMA," *Chemical Engineering Journal*, vol. 179, pp. 140–150, 2012.

[21] S. Dultz, J.-H. An, and B. Riebe, "Organic cation exchanged montmorillonite and vermiculite as adsorbents for Cr(VI): effect of layer charge on adsorption properties," *Applied Clay Science*, vol. 67-68, pp. 125–133, 2012.

[22] Z. Ghasemi, I. Sourinejad, H. Kazemian, M. Hadavifar, S. Rohani, and H. Younesi, "Kinetics and thermodynamic studies of Cr(VI) adsorption using environmental friendly multifunctional zeolites synthesized from coal fly ash under mild conditions," *Chemical Engineering Communications*, vol. 207, no. 6, pp. 808–825, 2019.

[23] X.-y. Zou, F. Xiao, S.-r. Liu et al., "Preparation and application of CPC/Keggin-Al_{30} modified montmorillonite composite for Cr (VI) removal," *Journal of Water Process Engineering*, vol. 37, p. 101348, 2020.

[24] S. Liu, M. Chen, X. Cao et al., "Chromium (VI) removal from water using cetylpyridinium chloride (CPC)-modified montmorillonite," *Separation and Purification Technology*, vol. 241, article 116732, 2020.

[25] M. C. Brum, J. L. Capitaneo, and J. F. Oliveira, "Removal of hexavalent chromium from water by adsorption onto surfactant modified montmorillonite," *Minerals Engineering*, vol. 23, no. 3, pp. 270–272, 2010.

[26] A. Atia, "Adsorption of chromate and molybdate by cetylpyridinium bentonite," *Applied Clay Science*, vol. 41, no. 1-2, pp. 73–84, 2008.

[27] J. Chanra, E. Budianto, and B. Soegijono, "Surface modification of montmorillonite by the use of organic cations via conventional ion exchange method," *IOP Conference Series: Materials Science and Engineering*, vol. 509, article 012057, 2019.

[28] J. Nones, J. Nones, A. Poli, A. G. Trentin, H. G. Riella, and N. C. Kuhnen, "Organophilic treatments of bentonite increase the adsorption of aflatoxin B_1 and protect stem cells against cellular damage," *Colloids and Surfaces. B, Biointerfaces*, vol. 145, pp. 555–561, 2016.

[29] J. D. Castro-Castro, I. F. Macías-Quiroga, G. I. Giraldo-Gómez, and N. R. Sanabria-González, "Adsorption of Cr(VI) in aqueous solution using a surfactant-modified bentonite," *Scientific World Journal*, vol. 2020, p. 3628163, 2020.

[30] A. Ayub, Z. A. Raza, M. I. Majeed, M. R. Tariq, and A. Irfan, "Development of sustainable magnetic chitosan biosorbent beads for kinetic remediation of arsenic contaminated water," *International Journal of Biological Macromolecules*, vol. 163, pp. 603–617, 2020.

[31] K. G. Akpomie and F. A. Dawodu, "Potential of a low-cost bentonite for heavy metal abstraction from binary component system," *Beni-Suef University Journal of Basic and Applied Sciences*, vol. 4, no. 1, pp. 1–13, 2015.

[32] M. I. Temkin, "Kinetics of ammonia synthesis on promoted iron catalysts," *Acta Physiochim. URSS*, vol. 12, pp. 327–356, 1940.

[33] W. Weber and J. Morris, "Kinetics of adsorption on carbon from solution," *Journal of the Sanitary Engineering Division*, vol. 89, no. 2, pp. 31–59, 1963.

[34] B. Ravel and M. Newville, "ATHENA,ARTEMIS,HEPHAESTUS: data analysis for X-ray absorption spectroscopy usingIFEFFIT," *Journal of Synchrotron Radiation*, vol. 12, no. 4, pp. 537–541, 2005.

[35] B. Sarkar, Y. Xi, M. Megharaj, G. S. R. Krishnamurti, D. Rajarathnam, and R. Naidu, "Remediation of hexavalent chromium through adsorption by bentonite based Arquad® 2HT-75 organoclays," *Journal of Hazardous Materials*, vol. 183, no. 1-3, pp. 87–97, 2010.

[36] L. F. de Magalhães, G. R. da Silva, and A. E. C. Peres, "Zeolite application in wastewater treatment," *Adsorption Science & Technology*, vol. 2022, pp. 1–26, 2022.

[37] B. Hu and H. Luo, "Adsorption of hexavalent chromium onto montmorillonite modified with hydroxyaluminum and

cetyltrimethylammonium bromide," *Applied Surface Science*, vol. 257, no. 3, pp. 769–775, 2010.

[38] K. G. Akpomie and F. A. Dawodu, "Acid-modified montmorillonite for sorption of heavy metals from automobile effluent," *Beni-Suef University Journal of Basic and Applied Sciences*, vol. 5, no. 1, pp. 1–12, 2016.

[39] A. G. Kumi, M. G. Ibrahim, M. Fujii, and M. Nasr, "Petrochemical wastewater treatment by eggshell modified biochar as adsorbent: atechno-economic and sustainable approach," *Adsorption Science & Technology*, vol. 2022, pp. 1–13, 2022.

[40] A. Pasgar, A. Nasiri, and N. Javid, "Single and competitive adsorption of Cu^{2+} and Pb^{2+} by tea pulp from aqueous solutions," *Environmental Health Engineering and Management*, vol. 9, pp. 65–74, 2022.

[41] N. K. Soliman and A. F. Moustafa, "Industrial solid waste for heavy metals adsorption features and challenges; a review," *Journal of Materials Research and Technology*, vol. 9, no. 5, pp. 10235–10253, 2020.

[42] J. Ren, F. Tao, and Y. Cui, "L-Glutamic acid crosslinked cellulose ester films for heavy metal ions adsorption," *Journal of Polymers and the Environment*, vol. 28, no. 4, pp. 1302–1314, 2020.

[43] T. Fan, M. Wang, X. Wang et al., "Experimental study of the adsorption of nitrogen and phosphorus by natural clay minerals," *Adsorption Science & Technology*, vol. 2021, pp. 1–14, 2021.

[44] X. Huang, L. Kong, S. Huang, M. Liu, and L. Li, "Synthesis of novel magnetic sulfur-doped Fe_3O_4 nanoparticles for efficient removal of Pb(II)," *SCIENCE CHINA Chemistry*, vol. 61, no. 2, pp. 164–171, 2018.

[45] W. Yao, Y. Wu, H. Pang, X. Wang, S. Yu, and X. Wang, "In-situ reduction synthesis of manganese dioxide@polypyrrole core/shell nanomaterial for highly efficient enrichment of U (VI) and Eu(III)," *SCIENCE CHINA Chemistry*, vol. 61, no. 7, pp. 812–823, 2018.

[46] N. Mabungela, N. D. Shooto, F. Mtunzi, and E. B. Naidoo, "The adsorption of copper, lead metal ions, and methylene blue dye from aqueous solution by pure and treated fennel seeds," *Adsorption Science & Technology*, vol. 2022, pp. 1–21, 2022.

[47] M. M. Meimand, N. Javid, and M. Malakootian, "Adsorption of sulfur dioxide on clinoptilolite/nano iron oxide and natural clinoptilolite," *Health Scope*, vol. 8, no. 2, p. 8, 2019.

[48] N. Javid, Z. Honarmandrad, and M. Malakootian, "Ciprofloxacin removal from aqueous solutions by ozonation with calcium peroxide," *Desalination and Water Treatment*, vol. 174, pp. 178–185, 2020.

[49] Z. Honarmandrad, N. Javid, and M. Malakootian, "Removal efficiency of phenol by ozonation process with calcium peroxide from aqueous solutions," *Science*, vol. 11, no. 2, 2021.

[50] J. Yang, B. Huang, and M. Lin, "Adsorption of hexavalent chromium from aqueous solution by a chitosan/bentonite composite: isotherm, kinetics, and thermodynamics studies," *Journal of Chemical & Engineering Data*, vol. 65, no. 5, pp. 2751–2763, 2020.

[51] J. Zhou, P. Wu, Z. Dang et al., "Polymeric Fe/Zr pillared montmorillonite for the removal of Cr(VI) from aqueous solutions," *Chemical Engineering Journal*, vol. 162, no. 3, pp. 1035–1044, 2010.

[52] A. Tytłak, P. Oleszczuk, and R. Dobrowolski, "Sorption and desorption of Cr(VI) ions from water by biochars in different environmental conditions," *Environmental Science and Pollution Research*, vol. 22, no. 8, pp. 5985–5994, 2015.

[53] J. Bayuo, M. A. Abukari, and K. B. Pelig-Ba, "Desorption of chromium (VI) and lead (II) ions and regeneration of the exhausted adsorbent," *Applied Water Science*, vol. 10, no. 7, p. 171, 2020.

[54] M. S. Slimani, H. Ahlafi, H. Moussout, F. Boukhlifi, and O. Zegaoui, "Adsorption of hexavalent chromium and phenol onto bentonite modified with hexadecyltrimethylammonium bromide (HDTMABr) council for innovative research," *Journal of Advances in Chemistry*, vol. 8, no. 2, pp. 1602–1611, 2014.

[55] R. Leyva-Ramos, A. Jacobo-Azuara, O. L. Torres-Rivera, R. M. Guerrero-Coronado, M. S. Berber-Mendoza, and P. Alonso-Davila, "Adsorption of chromium (VI) from water solution onto organobentonite," *Journal of Environmental Engineering and Management*, vol. 18, no. 5, pp. 311–317, 2008.

[56] C. Tan, S. Avasarala, and H. Liu, "Hexavalent chromium release in drinking water distribution systems: new insights into zerovalent chromium in iron corrosion scales," *Environmental Science & Technology*, vol. 54, no. 20, pp. 13036–13045, 2020.

[57] Y. Li, J. Li, and Y. Zhang, "Mechanism insights into enhanced Cr(VI) removal using nanoscale zerovalent iron supported on the pillared bentonite by macroscopic and spectroscopic studies," *Journal of Hazardous Materials*, vol. 227-228, pp. 211–218, 2012.

[58] A. A. Jock, I. O. Oboh, U. E. Inyang, L. P. Ganchok, and O. Adeku, "Chromium and nickel metal ions removal from contaminated water using Nigerian bentonite clay," *Water Practice and Technology*, vol. 16, no. 3, pp. 825–836, 2021.

[59] L. de Pablo, M. L. Chávez, and M. Abatal, "Adsorption of heavy metals in acid to alkaline environments by montmorillonite and Ca-montmorillonite," *Chemical Engineering Journal*, vol. 171, no. 3, pp. 1276–1286, 2011.

[60] B. S. Krishna, D. S. R. Murty, and B. S. Jai Prakash, "Surfactant-modified clay as adsorbent for chromate," *Applied Clay Science*, vol. 20, no. 1-2, pp. 65–71, 2001.

[61] P. Sannasi and D. Sathiaselvan, "Characterizing chromium (VI) removal mechanism by raw leaf powder of local 'Gapis' (Saraca thaipingensis) tree for use as biosorbent," in *In 6th International Conference on Environment (ICENV2018): Empowering Environment and Sustainable Engineering Nexus Through Green Technology*, Penang, Malaysia AIP Publishing, 2019.

[62] Y.-H. Chen, D.-Y. Liu, and J.-F. Lee, "Study of Cr(VI) adsorption onto magnetite nanoparticles using synchrotron-based X-ray absorption spectroscopy," *Physics and Chemistry of Minerals*, vol. 45, no. 9, pp. 907–913, 2018.

[63] P. Wu, S. Li, L. Ju et al., "Mechanism of the reduction of hexavalent chromium by organo-montmorillonite supported iron nanoparticles," *Journal of Hazardous Materials*, vol. 219-220, pp. 283–288, 2012.

[64] L. Sala and J. González, "Thermodynamic and dynamic of chromium biosorption by pectic and lignocellulocic biowastes," *Journal of Water Resource and Protection*, vol. 2, no. 10, pp. 888–897, 2010.

[65] Q. H. Pei, S. Shahir, L. Tao, and W. A. Ahmad, "Determination of chromium(VI) reduction by Acinetobacter haemolyticus using X-ray absorption fine structure spectroscopy," *Malaysian Journal of Fundamental and Applied Sciences*, vol. 4, no. 2, pp. 415–422, 2008.

[66] A. Dutta and N. Singh, "Surfactant-modified bentonite clays: preparation, characterization, and atrazine removal," *Environmental Science and Pollution Research*, vol. 22, no. 5, pp. 3876–3885, 2015.

[67] P. Pandey and N. De, "Surfactant-induced changes in physicochemical characters of bentonite clay," *International Research Journal of Pure and Applied Chemistry*, vol. 15, no. 4, pp. 1–11, 2018.

[68] N. Banik, S. A. Jahan, S. Mostofa et al., "Synthesis and characterization of organoclay modified with cetylpyridinium chloride," *Bangladesh Journal of Scientific and Industrial Research*, vol. 50, no. 1, pp. 65–70, 2015.

[69] M. F. Zawrah, R. M. Khattab, E. M. Saad, and R. A. Gado, "Effect of surfactant types and their concentration on the structural characteristics of nanoclay," *Spectrochimica Acta Part A: Molecular and Biomolecular Spectroscopy*, vol. 122, pp. 616–623, 2014.

[70] M. A. Abdel-Wahhab, E. S. El-Denshary, A. A. El-Nekeety et al., "Efficacy of organo-modified nano montmorillonite to protect against the cumulative health risk of aflatoxin B₁ and ochratoxin A in rats," *Soft Nanoscience Letters*, vol. 5, no. 2, pp. 21–35, 2015.

[71] J. Nones, J. Nones, H. G. Riella, N. C. Kuhnen, and A. Trentin, "Bentonite protects neural crest stem cells from death caused by aflatoxin B_1," *Applied Clay Science*, vol. 104, pp. 119–127, 2015.

[72] M. Andrunik and T. Bajda, "Modification of bentonite with cationic and nonionic surfactants: structural and textural features," *Materials (Basel)*, vol. 12, no. 22, pp. 1–22, 2019.

[73] N. Latifi, F. Vahedifard, E. Ghazanfari, and A. S. A. Rashid, "Sustainable usage of calcium carbide residue for stabilization of clays," *Journal of Materials in Civil Engineering*, vol. 30, no. 6, p. 04018099, 2018.

[74] C. Bertagnolli and M. G. C. da Silva, "Characterization of Brazilian bentonite organoclays as sorbents of petroleum-derived fuels," *Materials Research*, vol. 15, no. 2, pp. 253–259, 2012.

[75] K. Taleb, I. Pillin, Y. Grohens, and S. Saidi-Besbes, "Gemini surfactant modified clays: effect of surfactant loading and spacer length," *Applied Clay Science*, vol. 161, pp. 48–56, 2018.

[76] A. Nuntiya, S. Sompech, S. Aukkaravittayapun, and J. Pumchusak, "The effect of surfactant concentration on the interlayer structure of organoclay," *Chiang Mai Journal of Science*, vol. 35, pp. 199–205, 2008.

[77] I. Ltifi, F. Ayari, D. B. Chehimi, and M. T. Ayadi, "Physicochemical characteristics of organophilic clays prepared using two organo-modifiers: alkylammonium cation arrangement models," *Applied Water Science*, vol. 8, no. 3, pp. 1–8, 2018.